Perturbation of the Hydrophobic Core of Lipid Bilayers by the Human Antimicrobial Peptide LL-37†

Katherine A. Henzler-Wildman,‡,⊥ Gary V. Martinez,§ Michael F. Brown,§ and A. Ramamoorthy*,‡

Department of Chemistry and Biophysics Research Division, University of Michigan, Ann Arbor, Michigan 48109, and Department of Chemistry, University of Arizona, Tucson, Arizona 85721

Received December 18, 2003; Revised Manuscript Received April 27, 2004

ABSTRACT: LL-37 is a cationic, amphipathic α-helical antimicrobial peptide found in humans that kills cells by disrupting the cell membrane. To disrupt membranes, antimicrobial peptides such as LL-37 must alter the hydrophobic core of the bilayer. Differential scanning calorimetry and deuterium (^{2}H) NMR experiments on acyl chain perdeuterated lipids demonstrate that LL-37 inserts into the hydrophobic region of the bilayer and alters the chain packing and cooperativity. The results show that hydrophobic interactions between LL-37 and the hydrophobic acyl chains are as important for the ability of this peptide to disrupt lipid bilayers as its electrostatic interactions with the polar headgroups. The ^{2}H NMR data are consistent with the previously determined surface orientation of LL-37 (Henzler Wildman, K. A., et al. (2003) *Biochemistry 42,* 6545) with an estimated 5−6 Å depth of penetration of the hydrophobic face of the amphipathic helix into the hydrophobic interior of the bilayer. LL-37 also alters the material properties of lipid bilayers, including the area per lipid, hydrophobic thickness, and coefficient of thermal expansion in a manner that varies with lipid type and temperature. Comparison of the effect of LL-37 on 1-palmitoyl-2-oleoyl-phosphatidylcholine (POPC-d_{31}) and 1,2-dimyristoyl-phosphatidylcholine (DMPC-d_{54}) at different temperatures demonstrates the importance of bilayer order in determining the type and extent of disordering and disruption of the hydrophobic core by LL-37. One possible explanation, which accounts for both the ^{2}H NMR data presented here and the known surface orientation of LL-37 under identical conditions, is that bilayer order influences the depth of insertion of LL-37 into the hydrophobic/hydrophilic interface of the bilayer, altering the balance of electrostatic and hydrophobic interactions between the peptide and the lipids.

The increasing prevalence of antibiotic resistance necessitates the development of new ways to combat bacterial infection. Antimicrobial peptides represent a promising means for meeting this challenge. Unlike current antibiotics, which interact strongly with specific target molecules such as proteins, most antimicrobial peptides act by a nonspecific mechanism and often kill cells by disrupting the plasma membrane (*1*−*3*). The hydrophobic core of the lipid bilayer provides a barrier between the aqueous environments inside and outside the cell that must be breached for membrane-active peptides to cause cell death. Insertion of a peptide into the lipid bilayer in a manner that disorders the lipid acyl chains results in a decrease in the ability of the bilayer to act as a barrier and permits leakage, whether through organized peptide−lipid pores or local defects. For instance, extensive mutational and calorimetry studies of magainins have shown that the extent of peptide insertion and lipid bilayer disruption depends on the hydrophobicity, hydrophobic moment, and angle subtended by the hydrophobic face of the peptide helix, regardless of the net charge of the membrane (*4*−*6*). These results confirm that the ability of the peptide to interact with the hydrophobic region of the lipid bilayer is crucial in determining the degree of peptide-induced loss in cell membrane integrity.

In this study, the effect of the human antimicrobial peptide LL-37 on the core of lipid bilayers is monitored using a combination of calorimetry and solid-state NMR. LL-37 is a 4.5 kDa cationic, amphipathic α-helical antimicrobial peptide with the sequence LLGDFFRKSKEKIGKEFKRIVQRIKDFLRNLVPRTES (*7*). It is known to have antimicrobial activity in vivo (*8*−*11*) and induces vesicle leakage and permeabilization of the inner and outer membranes of *Escherichia coli* cells in a dose-dependent manner at concentrations comparable to its minimum inhibitory concentration (MIC)[1] (*12*−*14*). Although LL-37 is highly charged (16 charged residues, net +6 at neutral pH), it is not as selective as some α-helical amphipathic antimicrobial peptides, with MICs ranging from 1 to 10 μM for a variety of Gram-positive and Gram-negative bacteria and hemolytic

† This research was partly supported by the NSF (CAREER development award to A.R.) and by the NIH (M.F.B.). K.A.H.-W. was a Howard Hughes Medical Institute Predoctoral Fellow, and G.V.M. was a NIH postdoctoral fellow.

* Corresponding author: Dr. A. Ramamoorthy, email ramamoor@umich.edu; phone (734) 647−6572; fax (734) 764−3323.

‡ University of Michigan.

⊥ Current address: Biochemistry Department, Brandeis University, Waltham, MA 02454.

§ University of Arizona.

[1] Abbreviations: MIC, minimum inhibitory concentration; DMPC, 1,2-dimyristoyl-phosphatidylcholine; POPC, 1-palmitoyl-2-oleoyl-phosphatidylcholine; POPG, 1-palmitoyl-2-oleoyl-phosphatidylglycerol; DSC, differential scanning calorimetry; MLV, multilamellar vesicles.

10.1021/bi036284s CCC: $27.50
Published on Web 06/12/2004

activity occurring at 25 μM in vitro (*12*, *15*−*17*). This is consistent with an important role for hydrophobic peptide−lipid interactions in the mechanism of LL-37 activity, which balance the electrostatic interactions that promote antimicrobial selectivity. Previous studies have shown that the amphipathic helix of LL-37 lies parallel to the membrane surface, and ^{31}P NMR and differential scanning calorimetry (DSC) experiments reveal that LL-37 induces positive curvature strain but does not break the membrane into small fragments or micelles (*18*). The role of curvature strain has been discussed previously with regard to lipid modulation of membrane function (*19*, *20*). These results support a toroidal pore model of bilayer disruption or formation of less organized transient defects in the membrane. Thus, penetration into and interference with the hydrophobic interior of the lipid bilayer is expected to be important for LL-37 activity.

To better understand the mechanism of LL-37 activity, this work has investigated the effect of LL-37 on the hydrophobic acyl chain region of lipid bilayers using solid-state ^{2}H NMR and DSC. The DSC results demonstrate that LL-37 penetrates into the hydrophobic interior of the bilayer and disrupts acyl chain packing and cooperativity. While calorimetry provides insight into the effect of a peptide on the thermodynamic properties of the bilayer, site-specific resolution and quantitative information on the influence of LL-37 on acyl chain motion is obtained from ^{2}H NMR spectra of acyl chain perdeuterated lipids (*21*). The ^{2}H NMR experiments show that LL-37 disorders the acyl chains and are used to characterize the extent of the perturbation at different depths in the hydrophobic core. The results are consistent with the amphipathic helix axis aligned parallel to the membrane surface at the hydrophobic/hydrophilic interface of the bilayer. In addition, the NMR data are analyzed to determine the effect of LL-37 on the material properties of the lipid bilayers (*19*), such as hydrophobic thickness, area per lipid, and coefficient of thermal expansion, since the effect of LL-37 varies greatly with its environment. Although LL-37 is a highly charged cationic peptide, it is still hydrophobic enough to penetrate into the core of zwitterionic lipid bilayers, which is consistent with its moderate selectivity. The ability of LL-37 to perturb the hydrophobic region of the membrane is critical for its membrane-disrupting cell-lytic activity. The results presented here demonstrate that the process is strongly influenced by properties of the lipid environment, thus providing insight into the mechanism of both activity and selectivity of LL-37.

EXPERIMENTAL PROCEDURES

Materials. Peptide synthesis and cleavage reagents were purchased from Applied Biosystems (Foster City, CA) and Aldrich (Milwaukee, WI), respectively. Fmoc-protected amino acids were from Advanced ChemTech (Louisville, KY), and isotopically labeled Fmoc-amino acids were from Cambridge Isotope Labs (Cambridge, MA). All the lipids were purchased from Avanti Polar Lipids (Alabaster, AL). Chloroform and methanol were from Aldrich (Milwaukee, WI), and all other reagents were from Fisher (Pittsburgh, PA).

Peptide Synthesis. LL-37, a 37 residue peptide (*7*), was synthesized on an ABI-431A (Applied Biosystems, Foster City, CA) peptide synthesizer using FastMoc chemistry with double coupling and double deprotection. Cleavage from the Ser(*t*-Bu)−Wang resin (Peptides International, Louisville, KY) to produce a free carboxylate at the C-terminus and deprotection were accomplished using trifluoroacetic acid and scavengers. Characterization of the peptides by mass spectrometry and analytical HPLC indicated that they had the correct molecular weight (4.5 kDa) and were >96% pure.

Sample Preparation. All of the peptide concentrations are reported as peptide/lipid mole ratio or are given in mole percent of peptide relative to the total moles of peptide plus lipid. Multilamellar vesicle (MLV) samples were prepared by mixing the desired amounts of peptide and lipid in 2:1 $CHCl_3$/MeOH. The peptide/lipid samples were dried under a stream of nitrogen and then under vacuum overnight to completely remove any residual solvent. Tris buffer (10 mM Tris, 100 mM NaCl, 2 mM EDTA, pH 7.4) was added to the MLV samples used for the DSC experiments to produce a final lipid concentration of 0.5 mg/mL DMPC or an equimolar concentration of 9:1 DMPC/DMPG or 8:2 DMPC/DMPG. The samples were vortexed for 2 min above the lipid phase transition temperature and freeze−thawed several times to ensure a uniform mixture of lipid and peptide. MLV samples for solid-state ^{2}H NMR experiments contained 50 mg of DMPC-d_{54} with or without 2 mol % LL-37 and were prepared by transferring the dry peptide/lipid mixture to an 8-mm OD glass tube and adding 50 wt % ^{2}H-depleted water (Aldrich, Milwaukee, WI). The samples were again vortexed and subjected to 8−10 freeze−thaw cycles. The glass tubes were cut off a short distance above the sample and sealed with Teflon stoppers, paraffin, and Parafilm. ^{31}P NMR chemical shift spectra were used to confirm that the lipids were in a well-hydrated uniform lamellar phase. All MLV samples were stored at −20 °C prior to use.

Differential Scanning Calorimetry. All buffers and samples were degassed under vacuum for 15 min before being loaded into the Nano-DSC II calorimeter (Calorimetry Sciences Corp., Provo, UT). The scan rate was 0.25 °C/min over the temperature range 5−42 °C with 10 min equilibration between scans. Initial heating and cooling scans of buffer alone were run before each sample to provide a baseline. The sample was loaded below the main phase transition temperature (T_m), and heating and cooling scans were run until subsequent heating scans produced identical results. DSC experiments were conducted with samples containing peptide/lipid mole ratios in the range 1:500 to 1:25 in DMPC, 4:1 DMPC/DMPG, or 9:1 DMPC/DMPG, as well as pure lipid samples with no peptide. The raw data were converted to molar heat capacity using the CPCalc program provided with the calorimeter, using the lipid concentration and molecular weight of each sample along with a partial specific volume of 0.956 mL/g (*22*). The total calorimetric enthalpies were calculated by integrating the peak areas after baseline subtraction.

^{2}H NMR Spectroscopy. ^{2}H NMR quadrupolar echo spectra of MLV samples of acyl chain perdeuterated lipids were obtained on a Bruker AMX-500 spectrometer using a home-built 8-mm solenoid coil probe. The samples contained about 45 mg of lipid. The ^{2}H frequency was 76.77 MHz, and the $\pi/2$ pulse width was 4.25 μs. The spectral width was 1 MHz, the delay between the two $\pi/2$ pulses was 45 μs, and an average of 2000 scans were acquired for each sample with

a 1 s recycle delay. The data were processed and de-Paked (*23*−*26*) to obtain the 0° aligned spectra using Matlab scripts (*27*). The quadrupolar splitting was determined directly from the de-Paked spectrum and used to calculate the order parameter, S_{CD}, using

$$\Delta\nu_Q = \frac{3}{4}\chi_Q(3\cos^2\theta - 1)S_{CD} \quad (1)$$

where $\theta = 0°$ and $\chi_Q = 167$ kHz (*28*) (in the de-Paked spectra, the average bilayer normal is parallel to the laboratory frame). Although S_{CD} is negative, it is reported as the absolute value in most figures. An oriented sample of POPC-d_{31} with 1% LL-37 was also prepared, and the spectrum with the bilayer normal parallel to the magnetic field (0° alignment) was compared with the de-Paked powder-type spectrum of an otherwise identical MLV sample to confirm the accuracy of the de-Pakeing procedure.

Smoothed order parameter profiles were determined for the POPC-d_{31} and 3:1 POPC-d_{31}/POPG spectra by integrating the area under the de-Paked spectra and dividing it into equal portions. Since the spectra are more complicated for DMPC-d_{54} due to perdeuteration of both acyl chains, the area under the peaks in the quadrupolar echo spectra was fit to determine the number of nuclei and then used in conjunction with previous assignments of site-specifically deuterated DMPC (*29*, *30*) to derive the order parameter profile. Although LL-37 changes the quadrupolar splitting, it does not change the overall shape of the spectra in any of the lipid types studied, allowing the peaks to be assigned with the reasonable assumption that the arrangement of peaks in the spectrum is not perturbed by the peptide. The site-specific change in S_{CD} between pure lipid and lipid plus peptide was then calculated as

$$\Delta S_{CD}^{(i)} = |S_{CD}^{(i)}(\text{lipid})| - |S_{CD}^{(i)}(\text{lipid+peptide})| \quad (2)$$

To enable comparison of the relative change in order parameter along the chain upon addition of peptide, the change in S_{CD} was normalized to that of the pure lipid,

$$\Delta S_{CD}^{(i),\text{norm}} = \frac{\Delta S_{CD}^{(i)}}{S_{CD}^{(i)}(\text{lipid})} \quad (3)$$

THEORETICAL BASIS

Analysis of Order Parameters Using the First-Order Mean-Torque Model. The mean-torque model is a continuum model of acyl chain segment orientations, naturally including molecular and bilayer motions in addition to acyl chain isomerization (*21*, *31*), and it has been shown to be superior to discrete models for configurational statistics of lipid bilayers (*32*, *33*). The use of the mean-torque model follows Petrache et al. (*21*), and only the key points are summarized here. The order parameter describing the motion of the *i*th segment with respect to the bilayer normal is given by

$$S_{CD}^{(i)} = \langle D_{00}^{(2)}(\Omega_{PN}^{(i)})\rangle \quad (4)$$

where $\mathbf{D}^{(2)}$ is the second-rank Wigner rotation matrix, $\Omega_{PN} = \beta_{PN}$ represents the angle between the C−D bond direction and the bilayer normal (*N* frame), and the angular brackets denote a time or ensemble average (*34*).

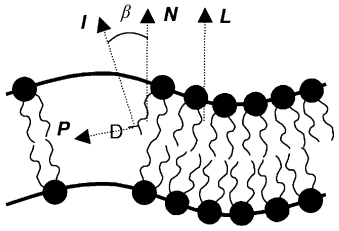

FIGURE 1: Frame transformations involved in order parameter analysis. *P* represents the frame of the principal axis system of the deuterium quadrupolar interaction, and the bilayer normal frame is indicated by *N*. *I* designates the internal frame. The laboratory frame, *L*, is defined by the magnetic field direction and is parallel to *N* for a 0°-oriented bilayer sample.

The segmental order parameter is subdivided using the rules for Wigner rotation matrix frame transformations (*34*) (see Figure 1), resulting in

$$S_{CD}^{(i)} = -\frac{1}{2}\left\langle\frac{3}{2}\cos^2\beta^{(i)} - \frac{1}{2}\right\rangle \quad (5)$$

where $\beta^{(i)}$ describes the orientation of the internal frame (*I*) of a particular segment with respect to the average bilayer normal (*N*). For a methylene group, the internal *z*-axis is perpendicular to the D−C−D plane; cf. Figure 1. The mean-torque model assumes that the orientational distribution of each acyl chain segment results from a mean-field orientational potential, which is expanded as a series of Legendre polynomials

$$U(\beta) = U_0P_0(\cos\beta) + U_1P_1(\cos\beta) + U_2P_2(\cos\beta) + ... \quad (6)$$

where the superscript *i* is suppressed for clarity. Here the coefficients, U_0, U_1, U_2, ..., depend on the position of the segment along the acyl chain, pressure, temperature, and bilayer hydration level. All the samples used in this work were prepared identically, so that the coefficients depend only on temperature and acyl chain position.

Petrache et al. (*21*) showed that the first-order mean-torque model is sufficient to describe the behavior of symmetric, saturated acyl chain bilayers, such as DMPC-d_{54} in the L_α phase. Assuming a Boltzmann distribution, the first-order mean-torque coefficients U_1 are calculated from

$$S_{CD} = -\frac{1}{2}\frac{\int_0^\pi\left(\frac{3}{2}\cos^2\beta - \frac{1}{2}\right)e^{-U(\beta)/kT}\sin\beta\,d\beta}{\int_0^\pi e^{-U(\beta)/kT}\sin\beta\,d\beta} = -\frac{1}{2} - \frac{3k^2T^2}{2U_1^2} + \frac{3kT}{2U_1}\coth\left(\frac{U_1}{kT}\right) \quad (7)$$

The average projection of each segment onto the bilayer normal,

$$l = l_0\langle\cos\beta\rangle \quad (8)$$

can then be calculated in a similar manner using the known potential function, where $l_0 = 1.27$ Å is the maximum segmental projection along the bilayer normal.

Area per Lipid and Coefficient of Thermal Expansion. Calculation of the area per lipid from the total acyl chain length obtained by summing these projections is complicated,

because it assumes (*33*)

$$1/\langle L\rangle \approx \langle 1/L\rangle \tag{9}$$

Therefore, following ref *21*, calculation of the acyl chain length and hydrophobic thickness of the bilayer is done using a second-order expansion of

$$q \equiv \langle 1/\cos\beta\rangle \tag{10}$$

near the point of maximum probability, which provides a better approximation than eq 9,

$$q \approx 3 - 3\langle\cos\beta\rangle + \langle\cos^2\beta\rangle \tag{11}$$

where the first and second moments are calculated from the previously determined potential function, cf. eq 7. Moreover, only the plateau order parameters are used in the calculation to avoid complications from chain upturns, early terminations, and interdigitation. The final results for calculation of the area and the hydrophobic thickness of one monolayer of the bilayer are

$$\langle A\rangle = \frac{2qV_{CH_2}}{l_0} \tag{12}$$

$$D_C = \frac{2V_C}{\langle A\rangle} = \frac{n_C l_0}{q} \tag{13}$$

in which n_C is the number of carbons per acyl chain (14 for DMPC); V_{CH_2} and V_C are the volume per methylene and hydrocarbon volume per lipid chain, respectively, and are estimated as described (*21*).

The coefficient of thermal expansion,

$$\alpha = \frac{1}{V}\left(\frac{\partial V}{\partial T}\right)_P \tag{14}$$

can be divided into components parallel and perpendicular to the bilayer normal. Since the hydrocarbon thickness and area per lipid are inversely related,

$$\alpha = \frac{1}{D_C}\left(\frac{\partial D_C}{\partial T}\right)_P + \frac{1}{\langle A\rangle}\left(\frac{\partial\langle A\rangle}{\partial T}\right)_P \tag{15}$$

$$\alpha = \alpha_{\parallel} + \alpha_{\perp} \tag{16}$$

The coefficients of thermal expansion, calculated according to these equations, describe the rate of change of the area per lipid or hydrocarbon thickness of a lipid bilayer as a function of temperature.

RESULTS

Differential Scanning Calorimetry of Lipid Mixtures with LL-37. The effect of LL-37 on the thermotropic phase behavior of DMPC and 4:1 DMPC/DMPG multilamellar vesicles hydrated with Tris buffer was observed using differential scanning calorimetry (DSC). DSC heating scans of the gel to liquid crystalline (L_α) phase transition of the lipids alone and with increasing LL-37 concentrations are shown in Figure 2. In the pure lipid scans, there is a tall narrow peak near 24 °C corresponding to the chain melting transition (rippled gel, P_β', to fluid lamellar, L_α), which has a large enthalpy and is highly cooperative. There is also a smaller, broader peak near 13 °C corresponding to the pretransition (lamellar gel, L_β', to rippled gel, P_β'). The pretransition has a lower enthalpy, is less cooperative, and corresponds to melting or untilting of the lipid headgroup. The width of the transition peak in the DSC scan, reported as $\Delta T_{1/2}$, is inversely related to the cooperativity of the transition, so a narrower peak corresponds to a larger cooperative unit. There is a slight difference in the enthalpy of the main phase transition (ΔH), the temperature of the main phase transition (T_m), and the cooperativity of the pretransition between the DMPC and 4:1 DMPC/DMPG samples. However, both show the features characteristic of a pure lipid or ideal lipid mixture. Further discussion of the phase transitions of pure saturated phosphatidylcholines, phosphatidylglycerols, and their binary mixtures can be found elsewhere (*35*−*37*).

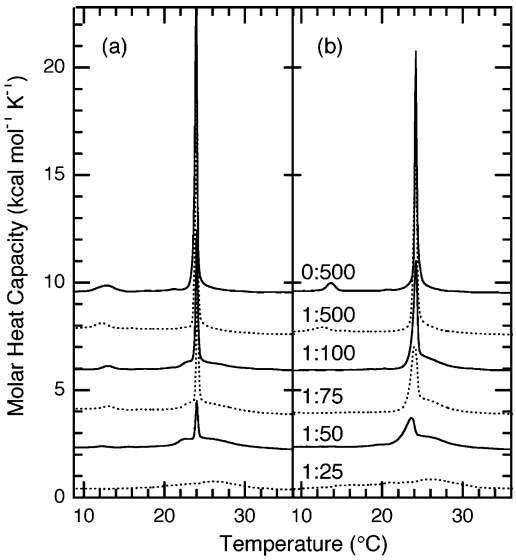

FIGURE 2: DSC heating scans of the main phase transition as a function of LL-37 concentration: (a) DMPC; (b) 4:1 DMPC/DMPG with LL-37/lipid mole ratios as indicated. For clarity, the traces are offset and alternating solid and dashed lines are used. In both DMPC and 4:1 DMPC/DMPG, LL-37 decreases the cooperativity of the main phase transition, indicating that it disrupts the packing of the lipid acyl chains.

The effect of varying amounts of LL-37 on both the pretransition and main transition of DMPC and 4:1 DMPC/DMPG are also shown in the DSC heating scans in Figure 2. As the concentration of LL-37 increases, the pretransition peak disappears, and the melting of the acyl chains becomes less cooperative as demonstrated by the decreasing amplitude and increasing width ($\Delta T_{1/2}$) of the main transition peak. At the lower LL-37 concentrations, the shape of the main transition peak is very similar to that of the pure lipid, but at higher LL-37 concentrations, it becomes asymmetric. The asymmetric line shape indicates that the phase transition is no longer two-state or there are multiple two-state transitions. Making the reasonable assumption that there are two phases that coexist and each undergoes a two-state transition, the low, broad component is attributed to lipids in peptide-rich regions or those lipids that are near the peptide and are highly perturbed. The sharper peak is more similar to the peak observed for pure lipids and is attributed to those lipids that are in peptide-poor regions or are farther away from the peptide and thus have less perturbed acyl chains.

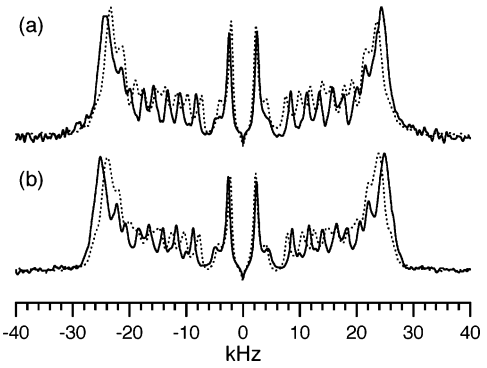

FIGURE 3: Effect of LL-37 on the ^{2}H NMR spectrum of POPC-d_{31}: (a) POPC-d_{31} bilayers; (b) 3:1 POPC-d_{31}/POPG bilayers. The pure lipid spectra are shown as solid lines, and the spectra in the presence of 1% LL-37 are shown as dotted lines. All the spectra are de-Paked quadrupolar echo spectra of randomly oriented lipid bilayer dispersions at 35 °C. LL-37 causes a decrease in the quadrupolar splittings of POPC-d_{31}, both alone and when mixed with POPG. Thus, LL-37 increases the disorder in both zwitterionic and anionic bilayers containing this lipid.

The effect of LL-37 on zwitterionic (DMPC, Figure 2a) and anionic (4:1 DMPC/DMPG, Figure 2b) lipid bilayers is similar, but LL-37 is slightly more disruptive to the negatively charged bilayers. This is observed through the greater broadening and shift of temperature of the sharp component of the main phase transition in the presence of LL-37 in the anionic lipid mixture. The pretransition also disappears at lower LL-37 concentrations in the 4:1 DMPC/DMPG mixture than in pure DMPC. The total enthalpy of the main phase transition decreases slightly in both DMPC and 4:1 DMPC/DMPG, but it does not go to zero, indicating that the phase transition is not abolished.

^{2}H Solid-State NMR Spectroscopy of Mixtures of POPC-d_{31} and POPC-d_{31}/POPG with LL-37. Solid-state ^{2}H NMR was used to investigate the effect of LL-37 on the lipid acyl chains in the L_α phase and to provide site-specific resolution of its influences on the hydrocarbon region. Quadrupolar echo ^{2}H NMR spectra of LL-37 in three different lipid environments (DMPC-d_{54}, POPC-d_{31}, and 3:1 POPC-d_{31}/POPG) and a range of temperatures were obtained. The powder-type spectra of the unoriented samples were numerically inverted (de-Paked) (*24*) to obtain the 0°-oriented spectra, which have greater resolution. Representative de-Paked ^{2}H NMR spectra of POPC-d_{31} at 35 °C alone and with 1 mol % LL-37 incorporated are shown in Figure 3a, and the corresponding spectra of 3:1 POPC-d_{31}/POPG with and without 1 mol % LL-37 are shown in Figure 3b. Since the ^{2}H NMR line shapes in the presence of LL-37 are similar to the pure lipid spectra (see Figure 3), the peaks in the spectra with LL-37 present were assigned in the same manner, as described in the Experimental Procedures section. ^{31}P NMR spectra of each sample confirmed that the lipids were in a fluid lamellar phase with a typical ^{31}P chemical shift powder pattern both before and after ^{2}H NMR experiments were performed (results not shown).

From the de-Paked ^{2}H NMR spectra (Figure 3), it is clear that the quadrupolar splittings decrease in the presence of LL-37, indicating that it causes disordering of the lipid acyl chains. The smoothed order parameter profiles for POPC-d_{31} with 0%, 1%, and 2% LL-37 incorporated are shown at several different temperatures in Figure 4a to more clearly

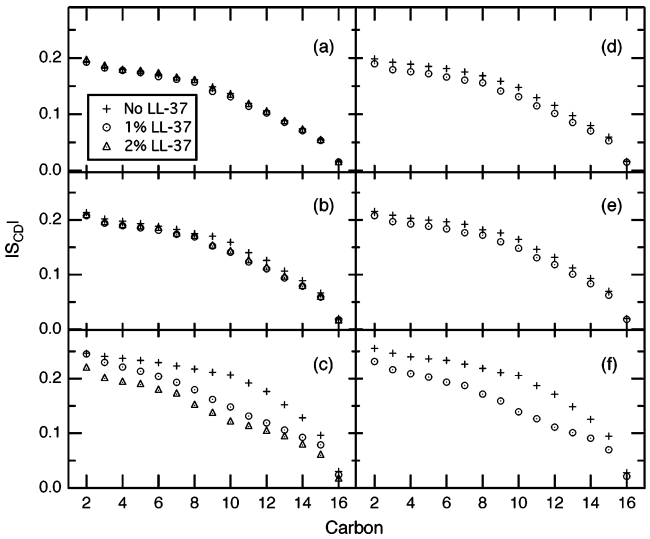

FIGURE 4: Effect of LL-37 on the order parameter profile of POPC-d_{31}. Smoothed order parameter profiles are shown for POPC-d_{31} bilayers at (a) 50, (b) 35, and (c) 10 °C; and for 3:1 POPC-d_{31}/POPG bilayers at (d) 50, (e) 35, and (f) 10 °C with the LL-37 concentrations indicated in the figure. LL-37 decreases the order parameters throughout the acyl chain in both types of bilayers with the greatest effect at 10 °C.

illustrate the effect of LL-37 at each temperature. Figure 4a−c shows that LL-37 causes a decrease in the value of $|S_{CD}|$ throughout the acyl chain in zwitterionic POPC-d_{31}, although the magnitude of the effect is much larger at lower temperatures than at higher temperatures. These profiles also show that acyl chain disruption increases with increasing peptide concentration, as is most easily seen by comparing the effect of 1% and 2% LL-37 on POPC-d_{31} at 10 °C, where the acyl chain disordering induced by LL-37 is largest. Figure 4d−f shows the corresponding order parameter profiles for 3:1 POPC-d_{31}/POPG with 0% or 1% LL-37 incorporated at the same temperatures. The results for the anionic POPC/POPG lipid mixture are very similar to those observed in zwitterionic POPC. The effect of LL-37 on both lipid systems appears similar, but there may be differences that do not appear in these data, since only the saturated acyl chain of the zwitterionic POPC component is perdeuterated and thus only this component is observed.

Although addition of LL-37 results in a decrease in the magnitude of the segmental order parameters in both lipid environments, its effect is not uniform along the acyl chain. To highlight this, order parameter difference profiles were calculated by subtracting the $|S_{CD}|$ values of the mixed peptide/lipid samples from the $|S_{CD}|$ results for the same acyl chain position in the pure lipid. With this convention, a positive value of ΔS_{CD} indicates a decrease in $|S_{CD}|$ (or increase in disorder) upon addition of LL-37. However, the difference profiles are complicated by the intrinsic decrease in the magnitude of the order parameters along the acyl chain. Thus, what appears as a small order parameter difference at the tail end of the acyl chain is actually a large change relative to its initial value in the pure lipid. To correct for this effect, the order parameter difference profiles are normalized relative to the pure lipid order parameter profile as shown in Figure 5. These profiles show the fractional change in order parameter upon incorporation of LL-37. They reveal that the extent of acyl chain disordering by LL-37 is

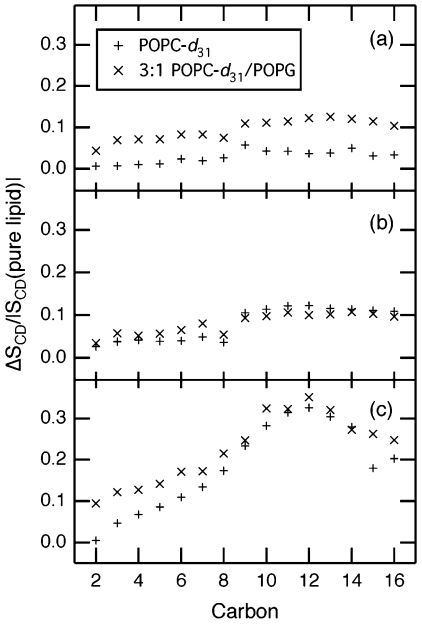

FIGURE 5: Normalized order parameter difference profiles upon addition of 1% LL-37 to POPC-d_{31} and 3:1 POPC-d_{31}/POPG at (a) 50, (b) 35, and (c) 10 °C. The normalized order parameter difference is calculated as described in the text and reflects the fractional change in $|S_{CD}|$ at each position along the acyl chain upon addition of LL-37. The values are positive, indicating that the presence of LL-37 induces a decrease in the order. The effect is much larger in the tail half of the acyl chain than near the headgroup.

divided into two distinct regions along the acyl chain. The upper half of the acyl chain (C2−C8) is disordered by LL-37, but the effect is much greater in the lower half of the acyl chain (C9−C16). Within each region the effect of LL-37 is relatively constant, and the same pattern along the acyl chain is observed at all temperatures and for both the zwitterionic and anionic lipid bilayers. This greater perturbation of the tail end of the acyl chain is consistent with a surface orientation of the LL-37 helix at the hydrophobic/hydrophilic interface, as determined previously (*18*), which is discussed below in more detail.

As the temperature increases, lipid bilayers naturally become more fluid and disordered, resulting in a decrease in order parameter with temperature. One possible explanation for the decreasing effect of LL-37 with increasing temperature is simply that a certain amount of disorder in the acyl chains is required to accommodate the insertion of the amphipathic helix, and at higher temperatures, the hydrophobic core is already sufficiently disordered so that the helix can insert with minimal additional effect on the acyl chains. To assess this hypothesis, it is useful to compare the order parameter profiles as a function of temperature instead of LL-37 concentration, and this is shown in Figure 6. The pure lipid profiles are shown in Figure 6, parts a and c, and the profiles in the presence of 1% LL-37 are shown in Figure 6, parts b and d. These graphs show that LL-37 suppresses the change in acyl chain order parameter with temperature, particularly in the tail half of the acyl chain (from C8/C9 to C16), supporting the proposed explanation for the temperature dependence of acyl chain disordering by LL-37.

^{2}H Solid-State NMR Spectroscopy of Mixtures of DMPC-d_{54} with LL-37. Quadrupolar echo ^{2}H NMR spectra of DMPC-d_{54} multilamellar vesicles with (dashed line) and

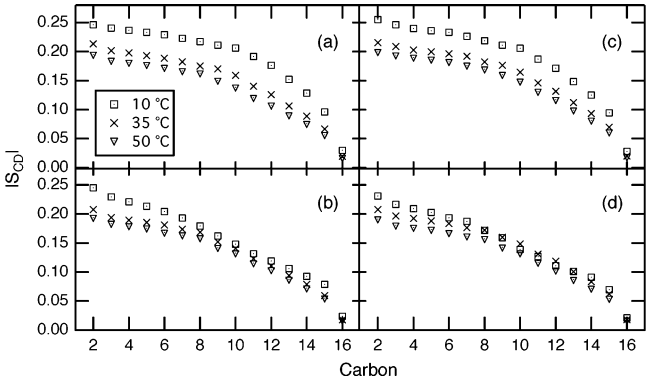

FIGURE 6: Effect of LL-37 on the order parameter profile of POPC-d_{31} as a function of temperature. Smoothed order parameter profiles are shown for (a) POPC-d_{31}; (b) POPC-d_{31} with 1% LL-37; (c) 3:1 POPC-d_{31}/POPG; and (d) 3:1 POPC-d_{31}/POPG with 1% LL-37 at 10, 35, and 50 °C as indicated in the figure. The presence of LL-37 suppresses the change in the lipid order parameters with temperature, particularly in the tail end of the acyl chain.

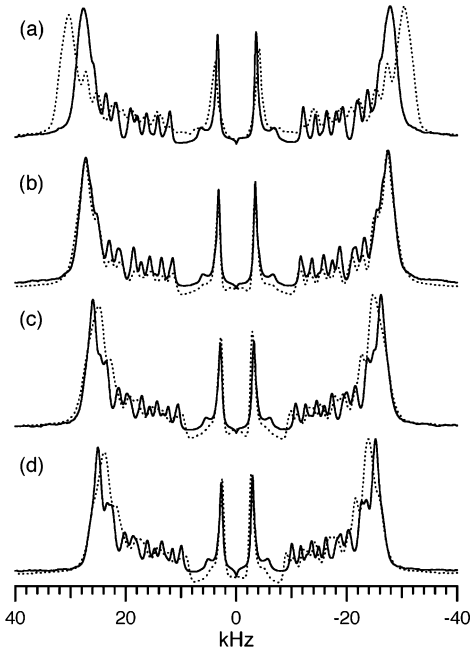

FIGURE 7: Effect of LL-37 on the ^{2}H NMR Spectra of DMPC-d_{54} bilayers. De-Paked quadrupolar echo spectra of unoriented DMPC-d_{54} bilayers in the absence (solid line) and presence (dotted line) of 2% LL-37 at (a) 35, (b) 40, (c) 45, and (d) 50 °C. At 45 and 50 °C, LL-37 induces a decrease in the quadrupolar splittings as was observed in POPC-d_{31}. LL-37 causes the opposite effect at 35 °C, and at 40 °C, the spectra in the presence and absence of LL-37 match.

without (solid line) 2% LL-37 were also obtained, as shown in Figure 7. The spectra of the random dispersions were de-Paked to obtain the 0°-oriented spectra (bilayer normal parallel to the magnetic field). At 35 °C (Figure 7a), the quadrupolar splitting is greater in the presence of LL-37 at all positions along the acyl chain, while at 40 °C (Figure 7b), the spectrum of DMPC-d_{54} containing LL-37 matches that of the pure lipid. At the higher temperatures of 45 °C (Figure 7c) and 50 °C (Figure 7d), a decrease of the quadrupolar splittings is induced by LL-37. The decrease in the quadrupolar splittings along the acyl chain when LL-37 is added to DMPC-d_{54} at the higher temperatures reflects a less-ordered bilayer. The greater acyl chain motion corresponds to a thinning of the bilayer with increased surface

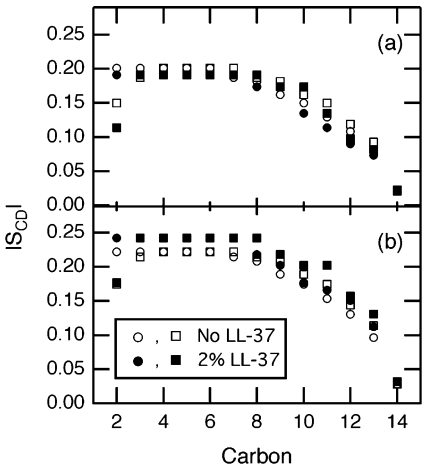

FIGURE 8: Effect of LL-37 on the order parameter profile of DMPC-d_{54} at (a) 50 and (b) 35 °C. The LL-37 concentration is indicated in the figure, and the *sn*-1 and *sn*-2 acyl chains are represented with circles and squares, respectively. The order parameters are larger in the presence of LL-37 at 35 °C but smaller in the presence of LL-37 at 50 °C.

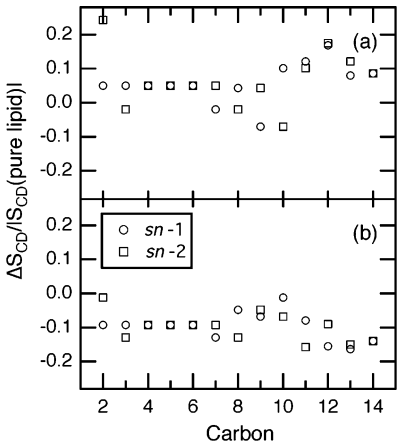

FIGURE 9: Normalized order parameter profiles for DMPC-d_{54} upon addition of 2% LL-37. The normalized order parameter difference is calculated as described in the text and is shown for (a) 50 and (b) 35 °C. These graphs show the fractional change in $|S_{CD}|$ at each position along both acyl chains upon addition of 2% LL-37. The positive values at 50 °C reflect an increase in disorder upon addition of LL-37, while the negative values at 35 °C reflect a decrease in disorder upon addition of LL-37 at that temperature. The effect is slightly larger near the tail end of the acyl chain than in the plateau region near the glycerol backbone.

area per lipid. This increased disorder induced by LL-37 in DMPC-d_{54} acyl chains at higher temperatures is similar to the effect of LL-37 on POPC-d_{31} and 3:1 POPC-d_{31}/POPG at all of the temperatures that were observed. However, the effect of LL-37 on DMPC-d_{54} at lower temperatures is opposite, for example, there is an increase in the quadrupolar splittings upon addition of LL-37 to DMPC-d_{54} at 35 °C, indicating a more-ordered or rigid bilayer with less acyl chain motion. This corresponds to a thicker bilayer with less surface area per lipid molecule, contrary to what might be expected for insertion of an amphipathic helix into the interface region of the bilayer. ^{15}N NMR experiments confirmed that the surface orientation of LL-37 is the same at all of these temperatures in DMPC and a variety of other lipids with the same 2% peptide concentrations (*18*). All of the temperatures studied are at least 10 °C above the gel to liquid-crystalline phase transition temperature of DMPC. The DSC results (Figure 2) show that even with the broadening of the transition, the lipids are fully in the liquid-crystalline phase at all of the temperatures and LL-37 concentrations used for the ^{2}H NMR experiments. A possible explanation for this unusual temperature dependence and behavior at 35 °C is discussed below, where these results are placed in context with the previously determined orientation of LL-37 and its effect on the lipid headgroups (*18*).

The order parameters along the acyl chain were determined based on the pure lipid assignments as described in the Experimental Procedures section and are shown in Figure 8a,b for the 35 and 50 °C data, respectively. Although LL-37 may either increase or decrease the order parameters, at a given temperature the direction of the change is generally consistent throughout the chain. The fractional change in order parameter upon addition of LL-37 is also slightly greater for the tail end of the acyl chain than for the portion near the glycerol backbone (Figure 9), as was observed in POPC-d_{31} and 3:1 POPC-d_{31}/POPG (Figure 5).

Influence of LL-37 on Bilayer Material Properties. As noted above, a reduction in quadrupolar splittings occurs naturally in pure lipids, such as DMPC-d_{54}, with increasing temperature due to greater motion of the acyl chains (*38*). This trend is evident in Figure 7, where it is also apparent that the quadrupolar splittings decrease even more dramatically with temperature in the LL-37 containing samples. This significant change in behavior with temperature is very different from what is observed in bilayers containing POPC-d_{31}, where the quadrupolar splittings and order parameter profiles have a smaller temperature variation in the presence of LL-37 (Figure 6). Thus, the effect of LL-37 on the lipid acyl chains is sensitive to their degree of saturation.

To describe the unusual effects of LL-37 on DMPC-d_{54} bilayers in a more quantitative manner, the order parameters were analyzed according to the first-order mean-torque model of Petrache et al. (*21*, *31*). Using this model, the order parameters were used to calculate the material properties of the DMPC-d_{54} bilayer in the presence and absence of LL-37. The influence of LL-37 on the hydrophobic thickness, area per lipid, and coefficient of thermal expansion were determined as described in the Experimental Procedures section. The area per lipid and monolayer hydrophobic thickness for DMPC-d_{54} alone and in the presence of 2% LL-37 are shown in Figure 10, which formulates the above observations quantitatively. At low temperatures, LL-37 thickens the bilayer and decreases the area per lipid, whereas it thins the bilayer and increases the area per lipid at higher temperatures. As a result, the changes in bilayer thickness and area as a function of temperature are increased in the presence of LL-37 relative to the normal behavior of the pure lipid. This property is described quantitatively by the coefficient of thermal expansion (*21*, *33*).

Values of the thermal expansion coefficients $\alpha_{\parallel}$ and $\alpha_{\perp}$ are shown in Figure 11 for DMPC with and without 2% LL-37. The figure shows that LL-37 increases the magnitude of the coefficient of thermal expansion both parallel and perpendicular to the bilayer normal. Although LL-37 increases the normal thinning of the bilayer with temperature, the effect of LL-37 on the thermal expansion coefficients decreases with temperature.

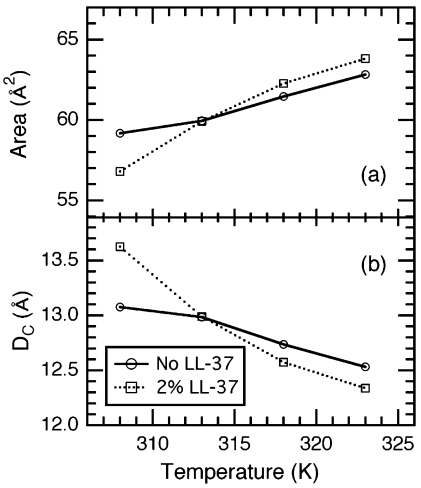

FIGURE 10: Area per lipid and hydrocarbon thickness of DMPC-d_{54}: (a) average cross-sectional area per lipid, calculated using eq 12; (b) half the bilayer hydrocarbon thickness, calculated using eq 13, for DMPC-d_{54} in the presence and absence of LL-37. Note that LL-37 increases the hydrocarbon thickness and decreases the area per lipid at low temperatures and has the opposite effect at high temperatures. The net effect is an increase in the rate of change of bilayer properties with temperature.

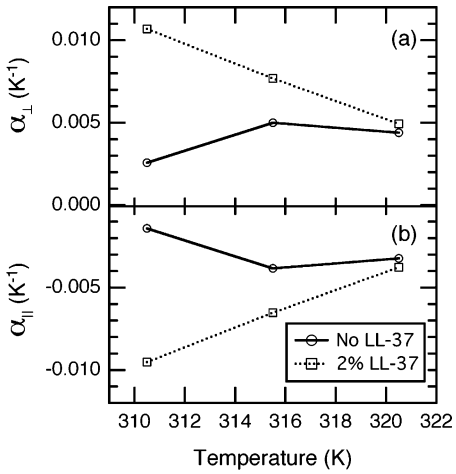

FIGURE 11: Coefficient of thermal expansion of DMPC-d_{54}: (a) perpendicular to the bilayer normal (change in area with temperature); (b) parallel to the bilayer normal (change in hydrocarbon thickness with temperature). LL-37 increases the magnitude of both the parallel and perpendicular components of the coefficient of thermal expansion.

DISCUSSION

LL-37 Disrupts Acyl Chain Packing and Cooperativity. Peptides that interact with membranes and perturb the lipid main phase transition have been divided into three classes (*39*−*42*). The classification is based on characteristic trends in the temperature (T_m), enthalpy (ΔH), and cooperativity ($\Delta T_{1/2}$) of the main phase transition induced by different types of peptides as a result of their profile and depth of insertion into the lipid bilayer. Type-1 peptides are cationic, water-soluble peptides, such as poly(L-lysine), which bind atmospherically to the polar membrane surface via electrostatic interactions. They cause no change or a slight increase in T_m and $\Delta T_{1/2}$ and a progressive increase in ΔH as peptide is added and have a greater effect on charged bilayers than zwitterionic bilayers. Type-2 peptides interact with the membrane through both electrostatic and hydrophobic effects and adsorb into the headgroup region, penetrating part way into the hydrophobic core of the bilayer and increasing vesicle permeability. Calorimetrically, they typically decrease T_m, increase $\Delta T_{1/2}$, and decrease ΔH with increasing peptide concentration and are sensitive to the presence of anionic lipids. Type-3 peptides are hydrophobic and insert deeply or span all the way across the hydrophobic core of the bilayer. They cause modest changes in T_m, increases in $\Delta T_{1/2}$, and large decreases in ΔH of the main phase transition and are insensitive to salt concentration, the presence of anionic lipids, and other electrostatic factors.

As a cationic, amphipathic α-helical peptide aligned on the surface of the bilayer, LL-37 fits the type-2 profile. In terms of its calorimetric behavior, LL-37 matches the type 2 prototype in that there is a large increase in $\Delta T_{1/2}$ with the formation of a peptide-perturbed broad component of the main phase transition and a general decrease in total enthalpy of the transition in both DMPC and 4:1 DMPC/DMPG. This is the expected behavior for a peptide that penetrates at least partway into the hydrophobic core of the bilayer, disrupting lipid−lipid contacts and preventing nearby lipids from undergoing the full chain-melting phase transition. However, the pattern of change in T_m upon peptide incorporation is more complex than that for a model type-2 peptide. Disordering of the lipid acyl chains due to intercalation of a type-2 peptide, as observed directly for LL-37 with the ^{2}H NMR experiments, is expected to favor the more fluid L_α phase and lead to a decrease in T_m of the peptide-perturbed regions. In contrast, the broad component of the DSC scans in the presence of LL-37, in both 4:1 DMPC/DMPG and DMPC, is centered a few degrees higher than the pure lipid T_m. In this regard, other type-2 surface-oriented peptides, including gramicidin S (*43*), δ-lysin (*44*), magainin (*45*), PGLa (*46*), and class A and L amphipathic α-helices (*47*), have been studied using DSC and show similar behavior to LL-37. This shift to higher T_m can be explained by electrostatic attraction between the peptide and the polar headgroups, which favors tighter packing of lipids in the gel phase and thus increases T_m. These results show that LL-37 behaves most like a type-2 peptide calorimetrically and emphasize the importance of both hydrophobic and hydrophilic forces in bilayer interaction and disruption by LL-37.

LL-37 Inserts into the Hydrophobic/Hydrophilic Interface of the Bilayer. Details on the depth at which LL-37 sits on the membrane surface are obtained from the ^{2}H NMR results. The decrease in order parameter of the POPC-d_{31} acyl chains upon incorporation of LL-37, with the largest effect in the core of the bilayer rather than near the polar/nonpolar interface, is consistent with an amphipathic peptide embedded on the bilayer surface as shown in Figure 12. This same pattern of perturbation of acyl chain order has been observed in ^{2}H NMR solid-state spectra of lipid bilayers with varying concentrations of other amphipathic peptides known to lie parallel to the membrane surface, including ovispirin (*48*), the P828 fragment of gp41 (*49*), and mastoparan X (*50*). In this model, the polar face of the amphipathic helix interacts with the lipid headgroups as observed by ^{31}P NMR (*18*), and the nonpolar face of the helix inserts into the hydrocarbon region, disrupting acyl chain packing and cooperativity as observed with both DSC and ^{2}H NMR. The presence of such a peptide within the bilayer interface increases the surface area, which results in a thinning of the bilayer and

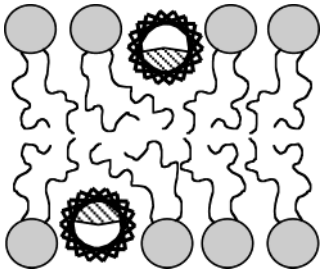

FIGURE 12: Schematic representation of LL-37 embedded in the hydrophobic/hydrophilic interface at the surface of the bilayer. The amphipathic helix is shown end on with the hydrophobic face shaded.

disordering effect on the acyl chains. Since the peptide only extends a short distance into the hydrophobic core of the bilayer, the effect of the increase in area per lipid is particularly pronounced in the region of the acyl chains that extends below the level of the peptide. The disordering of this lower portion of the acyl chains is greater than the plateau region because they must fill the volume between the hydrophobic face of the amphipathic helices and the opposite leaflet. In this way, empty space in the hydrophobic core of the bilayer is avoided. Assuming that the location of the discontinuity in the extent of LL-37-induced acyl chain disordering between C8 and C9 marks the bottom of the amphipathic helix, the order parameters of the top half of the acyl chain can be used to estimate the depth of insertion using a simple diamond-lattice model (*33*). On the basis of these parameters, the hydrophobic face of the LL-37 helix extends about 5−6 Å into the hydrophobic acyl chain region of the bilayer, which is consistent with half the diameter of an amphipathic helix.

The magnitude of bilayer disruption generally decreases with increasing temperature as observed in both the ^{31}P NMR spectra (*18*) and the ^{2}H NMR spectra. The disordering of the acyl chains is relatively constant in the presence of LL-37 for POPC-d_{31} regardless of temperature, in contrast to the normal decrease in order parameters with increasing temperature for pure lipids. As the acyl chains become more disordered, less adaptation is required for helix insertion, and perturbation of the acyl chain order in the presence of LL-37 is diminished at the higher temperatures. Very similar effects are observed in 3:1 POPC-d_{31}/POPG, supporting similar insertion of LL-37 at the polar/nonpolar interface of the bilayer in both zwitterionic and anionic lipid environments. These results emphasize the importance of hydrophobic interactions in addition to electrostatic attractions between the cationic peptide and the lipids.

LL-37 Insertion is Sensitive to Bilayer Composition. The interaction of LL-37 with the lipid headgroups was previously shown to differ between POPC and DMPC (*18*), and the ^{2}H NMR results presented here show that the interaction of LL-37 with the hydrophobic region of the bilayer is also sensitive to this difference. LL-37 disorders the acyl chains of DMPC at 45 and 50 °C, and this behavior is consistent with the expected effect of inserting a surface-parallel amphipathic helix into the hydrophobic/hydrophilic interface of the bilayer as discussed above (Figure 12). The DMPC-d_{54} spectra at 35 °C are more interesting, since LL-37 has the opposite effect, increasing the lipid acyl chain order, but the orientation of the peptide does not change over this temperature range (*18*). At the intermediate temperature of 40 °C, the spectra of DMPC-d_{54} in the presence and absence of LL-37 match. However, matching of the lipid bilayer properties to particular values preferred by the peptide would result in a decrease in the intrinsic temperature dependence of the lipid properties. Since LL-37 causes the opposite trend, namely, an increase in the change in lipid properties with temperature, the effect of LL-37 on the lipids cannot result from matching of the lipids to a set of properties preferred by the peptide.

Focusing only on the effect of LL-37 at 35 °C, cholesterol induces a similar increase in order parameters throughout the lipid acyl chains (*29, 30, 51*), but its effect is much larger and is the same at all temperatures, unlike LL-37. Such an increase in acyl chain order and corresponding decrease in area per lipid can also be caused by dehydration of the lipid bilayer or a change in headgroup conformation. This occurs upon binding of polyelectrolytes to the surface of oppositely charged bilayers (*52, 53*) due to the strong electrostatic interactions. Poly(lysine) is a highly cationic peptide that causes such an increase in acyl chain order upon membrane association (*52*), but poly(lysine) exhibits type-1 calorimetric behavior, and this was not observed for DMPC in the presence of LL-37. The calorimetric results demonstrate that LL-37 remains embedded in the membrane surface and does not switch to completely peripheral poly(lysine)-like binding above the surface of the lipid headgroups. However, LL-37 does have many charged residues along its length, including five lysine and six arginine residues, and the conformation of the DMPC headgroup is known to be sensitive to the charge at the bilayer surface (*54, 55*). Shallower insertion of LL-37 at 35 °C could alter the interaction between the peptide and the lipid headgroups and the bilayer surface charge, such that the dehydrating effect of the multiple charged residues becomes dominant. This slightly more peripheral binding of LL-37 could result from a combination of the high degree of ordering in DMPC at this temperature and the ability of LL-37 to self-associate. Most α-helical amphipathic antimicrobial peptides are unstructured in solution, but LL-37 is helical and aggregated, strongly suggesting that the hydrophobic face of the helix is buried upon self-association. The high surface area density of the saturated acyl chain lipid, DMPC, near the main transition temperature may disfavor insertion of LL-37 into the polar/nonpolar interface enough to shift the equilibrium of LL-37 insertion and aggregation. A more aggregated form of LL-37 with less hydrophobic surface area would insert less deeply into the bilayer, and this combined with a larger fraction of hydrophilic surface area would increase the electrostatic interaction between the peptide and the lipid headgroups. It is interesting to note that melittin, although it interacts differently with the bilayer and does not induce the same pattern of changes in the acyl chain order parameters, shows significantly different effects on the acyl chain order parameter profile of DMPC as a function of temperature (*56*). The high degree of ordering in the saturated acyl chain lipid, DMPC, near its gel to liquid crystalline phase transition temperature may result in a bilayer with such a high surface density that amphipathic peptides are restricted in how they can insert into the polar/nonpolar interface, resulting in behavior that is anomalous relative to more fluid bilayers. The ^{2}H NMR spectra of POPC-d_{31} and 3:1 POPC-d_{31}/POPG

indicate that LL-37 does not induce such behavior in monounsaturated bilayers, which have a greater area per lipid, even when comparably close to the main phase transition temperature. The ordering of the bilayer and area per lipid are therefore important in determining how LL-37 interacts with the membrane, its insertion depth, and its likely aggregation state.

Placing these results into the context of what is known about LL-37 from previously published work leads to a broader understanding of LL-37−lipid interaction. The DSC results presented here demonstrate that the perturbation induced by LL-37 is similar but not identical in DMPC and 4:1 DMPC/DMPG. This suggests that the electrostatic attraction between positively charged LL-37 and negatively charged DMPG changes the way the peptide sits in the membrane or alters its aggregation state, resulting in the observed differences in behavior in the DSC scans. Previously published ^{31}P NMR spectra indicate that headgroup perturbation is greater for 4:1 DMPC/DMPG than DMPC alone in water-hydrated samples (*18*). According to ^{15}N NMR spectra of site-specifically labeled LL-37 in oriented lipid bilayers, the LL-37 helix remains in the same surface orientation in both DMPC and 4:1 DMPC/DMPG at all temperatures (*18*). Thus, all the data fit best with a model where, in an anionic lipid environment, strong electrostatic interactions between the peptide and the lipid headgroups pull the helix higher into the hydrophilic region of the polar/nonpolar interface, as proposed by Dathe et al. (*4*, *6*, *57*). It follows that the perturbation of the lipid headgroups due to electrostatic interactions increases, whereas the depth of penetration of the peptide into the hydrophobic core of the lipid bilayer decreases. Thus, both the electrostatic interaction of LL-37 with the lipid headgroups and hydrophobic interaction with the acyl chain region of the bilayer affect the depth of insertion of LL-37 into the lipids and probably also affect its aggregation state on the bilayer surface, a property that is not well characterized.

LL-37 Alters the Material Properties of Lipid Bilayers. To characterize this unique behavior more quantitatively, several material properties of the bilayer were calculated from the order parameters using the first-order mean-torque model (*21*). These results show that LL-37 thickens the bilayer and decreases the area per lipid at low temperatures and has the opposite effect at high temperatures. LL-37 also increases the magnitude of both the parallel and perpendicular components (relative to the bilayer normal) of the coefficient of thermal expansion. This result is interesting since it is opposite of the normal effect of peptide matching in suppressing the natural change in bilayer properties with temperature.

These findings again show that the effect of LL-37 decreases with increasing temperature, and that the perturbation of DMPC-d_{54} is greater than for POPC-d_{31} at a given temperature. Although all of the bilayers studied are in the liquid crystalline phase, the bilayer order varies with temperature and degree of acyl chain unsaturation. The most disordered bilayers are the least perturbed by LL-37, and the more ordered bilayers are disrupted by the presence of the peptide. The effects of LL-37 on both the lipid headgroups (*18*) and acyl chains thus support a key role for bilayer configurational order in determining the extent of LL-37 insertion and the degree of bilayer perturbation.

ACKNOWLEDGMENT

We thank Horia Petrache for helpful discussions of the use of the mean-torque model.

REFERENCES

1. Koczulla, A. R., and Bals, R. (2003) Antimicrobial Peptides − Current Status and Therapeutic Potential, *Drugs 63*, 389−406.
2. Zasloff, M. (2002) Antimicrobial Peptides of Multicellular Organisms, *Nature 415*, 389−395.
3. Yeaman, M. R., and Yount, N. Y. (2003) Mechanisms of Antimicrobial Peptide Action and Resistance, *Pharmacol. Rev. 55*, 27−55.
4. Dathe, M., and Wieprecht, T. (1999) Structural Features of Helical Antimicrobial Peptides: Their Potential to Modulate Activity on Model Membranes and Biological Cells, *Biochim. Biophys. Acta 1462*, 71−87.
5. Giangaspero, A., Sandri, L., and Tossi, A. (2001) Amphipathic α Helical Antimicrobial Peptides − A Systematic Study of the Effects of Structural and Physical Properties on Biological Activity, *Eur. J. Biochem. 268*, 5589−5600.
6. Dathe, M., Meyer, J., Beyermann, M., Maul, B., Hoischen, C., and Bienert, M. (2002) General Aspects of Peptide Selectivity Towards Lipid Bilayers and Cell Membranes Studied by Variation of the Structural Parameters of Amphipathic Helical Model Peptides, *Biochim. Biophys. Acta 1558*, 171−186.
7. Gudmundsson, G. H., Agerberth, B., Odeberg, J., Bergman, T., Olsson, B., and Salcedo, R. (1996) The Human Gene FALL39 and Processing of the Cathelin Precursor to the Antibacterial Peptide LL-37 in Granulocytes, *Eur. J. Biochem. 238*, 325−332.
8. Di Nardo, A., Vitiello, A., and Gallo, R. L. (2003) Mast Cell Antimicrobial Activity is Mediated by Expression of Cathelicidin Antimicrobial Peptide, *J. Immunol. 170*, 2274−2278.
9. Nizet, V., Ohtake, T., Lauth, X., Trowbridge, J., Rudisill, J., Dorschner, R. A., Pestonjamasp, V., Piraino, J., Huttner, K., and Gallo, R. L. (2001) Innate Antimicrobial Peptide Protects the Skin from Invasive Bacterial Infection, *Nature 414*, 454−457.
10. Bals, R., Weiner, D. J., Moscioni, A. D., Meegalla, R. L., and Wilson, J. M. (1999) Augmentation of Innate Host Defense by Expression of a Cathelicidin Antimicrobial Peptide, *Infect. Immun. 67*, 6084−6089.
11. Bals, R., Weiner, D. J., Meegalla, R. L., and Wilson, J. M. (1999) Transfer of a Cathelicidin Peptide Antibiotic Gene Restores Bacterial Killing in a Cystic Fibrosis Xenograft Model, *J. Clin. Invest. 103*, 1113−1117.
12. Turner, J., Cho, Y., Dinh, N. N., Waring, A. J., and Lehrer, R. I. (1998) Activities of LL-37, a Cathelin-Associated Antimicrobial Peptide of Human Neutrophils, *Antimicrob. Agents Chemother. 42*, 2206−2214.
13. Oren, Z., Lerman, J. C., Gudmundsson, G. H., Agerberth, B., and Shai, Y. (1999) Structure and Organization of the Human Antimicrobial Peptide LL-37 in Phospholipid Membranes: Relevance to the Molecular Basis for its Non-Cell-Selective Activity, *Biochem. J. 341*, 501−513.
14. Zhao, C. Q., Nguyen, T., Boo, L. M., Hong, T., Espiritu, C., Orlov, D., Wang, W., Waring, A., and Lehrer, R. I. (2001) RL-37, an Alpha-Helical Antimicrobial Peptide of the *Rhesus* Monkey, *Antimicrob. Agents Chemother. 45*, 2695−2702.
15. Larrick, J. W., Hirata, M., Zhong, J., and Wright, S. C. (1995) Anti-microbial Activity of Human CAP18 Peptides, *Immunotechnology 1*, 65−72.
16. Johansson, J., Gudmundsson, G. H., Rottenberg, M. E., Berndt, K. D., and Agerberth, B. (1998) Conformation-Dependent Antibacterial Activity of the Naturally Occurring Human Peptide LL-37, *J. Biol. Chem. 273*, 3718−3724.
17. Tanaka, D., Miyasaki, K. Y., and Lehrer, R. I. (2000) Sensitivity of *Actinobacillus actinomycetemcomitans* and *Capnocytophaga spp*. to the Bactericidal Action of LL-37: A Cathelicidin Found in Human Leukocytes and Epithelium, *Oral Microbiol. Immunol. 15*, 226−231.
18. Henzler Wildman, K. A., Lee, D. K., and Ramamoorthy, A. (2003) Mechanism of Membrane Bilayer Disruption by the Human Antimicrobial Peptide, LL-37, *Biochemistry 42*, 6545−6558.
19. Brown, M. F. (1994) Modulation of Rhodopsin Function By Properties of the Membrane Bilayer, *Chem. Phys. Lipids 73*, 159−180.

20. Botelho, A. V., Gibson, N. J., Thurmond, R. L., Wang, Y., and Brown, M. F. (2002) Conformational Energetics of Rhodopsin Modulated by Nonlamellar-Forming Lipids, *Biochemistry 41*, 6354−6368.
21. Petrache, H. I., Dodd, S. W., and Brown, M. F. (2000) Area Per Lipid and Acyl Length Distributions in Fluid Phosphatidylcholines Determined by ^{2}H NMR Spectroscopy, *Biophys. J. 79*, 3172−3192.
22. Marsh, D. (1990) *CRC Handbook of Lipid Bilayers*, CRC Press, Ann Arbor, MI.
23. Bloom, M., Davis, J. H., and Mackay, A. L. (1981) Direct Determination of the Oriented Sample NMR-Spectrum from the Powder Spectrum for Systems with Local Axial Symmetry, *Chem. Phys. Lett. 80*, 198−202.
24. Sternin, E., Bloom, M., and Mackay, A. L. (1983) De-Pake-ing of NMR-Spectra, *J. Magn. Reson. 55*, 274−282.
25. McCabe, M. A., and Wassall, S. R. (1995) Fast-Fourier-Transform Depaking, *J. Magn. Reson. Ser. B 106*, 80−82.
26. McCabe, M. A., and Wassall, S. R. (1997) Rapid Deconvolution of NMR Powder Spectra by Weighted Fast Fourier Transformation, *Solid State Nucl. Magn. Reson. 10*, 53−61.
27. Martinez, G. V., Dykstra, E. M., Lope-Piedrafita, S., and Brown, M. F. (2004) Lanosterol and Cholesterol-Induced Variations in Bilayer Elasticity Probed by ^{2}H NMR Relaxation, *Langmuir 20*, 1043−1046.
28. Davis, J. H. (1983) The Description of Membrane Lipid Conformation, Order and Dynamics By ^{2}H-NMR, *Biochim. Biophys. Acta 737*, 117−171.
29. Oldfield, E., Meadows, M., Rice, D., and Jacobs, R. (1978) Spectroscopic Studies of Specifically Deuterium Labeled Membrane Systems. Nuclear Magnetic Resonance Investigation of Effects of Cholesterol in Model Systems, *Biochemistry 17*, 2727−2740.
30. Urbina, J. A., Pekerar, S., Le, H. B., Patterson, J., Montez, B., and Oldfield, E. (1995) Molecular Order and Dynamics of Phosphatidylcholine Bilayer- Membranes in the Presence of Cholesterol, Ergosterol and Lanosterol − a Comparative-Study Using ^{2}H-, ^{13}C- and ^{31}P-NMR Spectroscopy, *Biochim. Biophys. Acta 1238*, 163−176.
31. Petrache, H. I., Tu, K., and Nagle, J. F. (1999) Analysis of Simulated NMR Order Parameters for Lipid Bilayer Structure Determination, *Biophys. J. 76*, 2479−2487.
32. Salmon, A., Dodd, S. W., Williams, G. D., Beach, J. M., and Brown, M. F. (1987) Configurational Statistics of Acyl Chains in Polyunsaturated Lipid Bilayers From ^{2}H NMR, *J. Am. Chem. Soc. 109*, 2600−2609.
33. Jansson, M., Thurmond, R. L., Barry, J. A., and Brown, M. F. (1992) Deuterium NMR Study of Intermolecular Interactions in Lamellar Phases Containing Palmitoyllysophosphatidycholine, *J. Phys. Chem. 96*, 9532−9544.
34. Brown, M. F. (1996) Membrane Structure and Dynamics Investigated with NMR Spectroscopy, in *Membrane Structure and Dynamics* (Merz, K. M., and Roux, B., Eds.) pp 175−252, Birkhäuser, Boston, MA.
35. Findlay, E. J., and Barton, P. G. (1978) Phase Behavior of Synthetic Phosphatidylglycerols and Binary Mixtures With Phosphatidylcholines in the Presence and Absence of Calcium Ions, *Biochemistry 17*, 2400−2405.
36. Lewis, R. N. A. H., Mannock, D. A., and McElhaney, R. N. (1997) Membrane Lipid Molecular Structure and Polymorphism, *Curr. Top. Membr. 44*, 25−102.
37. Zhang, Y. P., Lewis, R., and McElhaney, R. N. (1997) Calorimetric and Spectroscopic Studies of the Thermotropic Phase Behavior of the n-Saturated 1,2-Diacylphosphatidylglycerols, *Biophys. J. 72*, 779−793.
38. Martinez, G. V., Dykstra, E. M., Lope-Piedrafita, S., Job, C., and Brown, M. F. (2002) NMR Elastometry of Fluid Membranes in the Mesoscopic Regime, *Phys. Rev. E 66*, 050902/1−050902/4.
39. Papahadjopoulos, D., Moscarello, M., Eylar, E. H., and Isac, T. (1975) Effects of Proteins On Thermotropic Phase Transitions of Phospholipid Membranes, *Biochim. Biophys. Acta 401*, 317−335.
40. McElhaney, R. N. (1982) The Use of Differential Scanning Calorimetry and Differential Thermal Analysis in Studies of Model and Biological-Membranes, *Chem. Phys. Lipids 30*, 229−259.
41. McElhaney, R. N. (1986) Differential Scanning Calorimetric Studies of Lipid−Protein Interactions in Model Membrane Systems, *Biochim. Biophys. Acta 864*, 361−421.
42. Lohner, K., and Prenner, E. J. (1999) Differential Scanning Calorimetry and X-ray Diffraction Studies of the Specificity of the Interaction of Antimicrobial Peptides with Membrane-Mimetic Systems, *Biochim. Biophys. Acta 1462*, 141−156.
43. Prenner, E. J., Lewis, R. N. A. H., Kondejewski, L. H., Hodges, R. S., and McElhaney, R. N. (1999) Differential Scanning Calorimetric Study of the Effect of the Antimicrobial Peptide Gramicidin S on the Thermotropic Phase Behavior of Phosphatidylcholine, Phosphatidylethanolamine and Phosphatidylglycerol Lipid Bilayer Membranes, *Biochim. Biophys. Acta 1417*, 211−223.
44. Lohner, K., Staudegger, E., Prenner, E. J., Lewis, R. N. A. H., Kriechbaum, M., Degovics, G., and McElhaney, R. N. (1999) Effect of *Staphylococcal* δ-Lysin on the Thermotropic Phase Behavior and Vesicle Morphology of Dimyristoylphosphatidylcholine Lipid Bilayer Model Membranes. Differential Scanning Calorimetric, ^{31}P Nuclear Magnetic Resonance and Fourier Transform Infrared Spectroscopic, and X- ray Diffraction Studies, *Biochemistry 38*, 16514−16528.
45. Matsuzaki, K., Harada, M., Funakoshi, S., Fujii, N., and Miyajima, K. (1991) Physicochemical Determinants For the Interactions of Magainins 1 and 2 With Acidic Lipid Bilayers, *Biochim. Biophys. Acta 1063*, 162−170.
46. Latal, A., Degovics, G., Epand, R. F., Epand, R. M., and Lohner, K. (1997) Structural Aspects of the Interaction of Peptidyl-Glycylleucine-carboxyamide, a Highly Potent Antimicrobial Peptide from Frog Skin, with Lipids, *Eur. J. Biochem. 248*, 938−946.
47. Mishra, V. K., Palgunachari, M. N., Segrest, J. P., and Anantharamaiah, G. M. (1994) Interactions of Synthetic Peptide Analogs of the Class a Amphipathic Helix With Lipids − Evidence For the Snorkel Hypothesis, *J. Biol. Chem. 269*, 7185−7191.
48. Yamaguchi, S., Huster, D., Waring, A., Lehrer, R. I., Kearney, W., Tack, B. F., and Hong, M. (2001) Orientation and Dynamics of an Antimicrobial Peptide in the Lipid Bilayer by Solid-State NMR Spectroscopy, *Biophys. J. 81*, 2203−2214.
49. Koenig, B. W., Ferretti, J. A., and Gawrisch, K. (1999) Site-Specific Deuterium Order Parameters and Membrane-Bound Behavior of a Peptide Fragment from the Intracellular Domain of HIV-1 gp41, *Biochemistry 38*, 6327−6334.
50. Whiles, J. A., Brasseur, R., Glover, K. J., Melacini, G., Komives, E. A., and Vold, R. R. (2001) Orientation and Effects of Mastoparan X on Phospholipid Bicelles, *Biophys. J. 80*, 280−293.
51. Trouard, T. P., Nevzorov, A. A., Alam, T. M., Job, C., Zajicek, J., and Brown, M. F. (1999) Influence of Cholesterol on Dynamics of Dimyristoylphosphatidylcholine Bilayers as Studied by Deuterium NMR Relaxation, *J. Chem. Phys. 110*, 8802−8818.
52. Laroche, G., Dufourc, E. J., Pezolet, M., and Dufourcq, J. (1990) Coupled Changes Between Lipid Order and Polypeptide Conformation at the Membrane Surface. A Deuterium NMR and Raman Study of Polylysine Phosphatidic-Acid Systems, *Biochemistry 29*, 6460−6465.
53. Huster, D., Dietrich, U., Gutberlet, T., Gawrisch, K., and Arnold, K. (2000) Lipid Matrix properties in Cationic Membranes Interacting with Anionic Polyelectrolytes: A Solid-State NMR Approach, *Langmuir 16*, 9225−9232.
54. Brown, M. F., and Seelig, J. (1977) Ion-Induced Changes in Headgroup Conformation of Lecithin Bilayers, *Nature 269*, 721−723.
55. Marassi, F. M., and Macdonald, P. M. (1992) Response of the Phosphatidylcholine Headgroup to Membrane Surface Charge in Ternary Mixtures of Neutral, Cationic, and Anionic Lipids: A Deuterium NMR Study, *Biochemistry 31*, 10031−10036.
56. Pott, T., Maillet, J. C., Abad, C., Campos, A., Dufourcq, J., and Dufourc, E. J. (2001) The Lipid Charge Density at the Bilayer Surface Modulates the Effects of Melittin on Membranes, *Chem. Phys. Lipids 109*, 209−223.
57. Dathe, M., Nikolenko, H., Meyer, J., Beyermann, M., and Bienert, M. (2001) Optimization of the Antimicrobial Activity of Magainin Peptides by Modification of Charge, *FEBS Lett. 501*, 146−150.

BI036284S